The 9th European Congress on Computational Methods in Applied Sciences and Engineering
ECCOMAS Congress 2024
3 – 7 June 2024, Lisboa, Portugal

STUDIES ON EFFECT OF INTERACTION OF COAXIAL JETS ON THRUST OF AIR-BREATHING ROCKET

TAKESHI SAWADA[*], AKIRA OYAMA[†], YUSUKE MARU[†] AND HIROYASU MANAKO [‡]

[*] The University of Tokyo
Hongo Bunkyo-ku 113-8654 Tokyo, Japan
e-mail: sawada-takeshi-78c@g.ecc.u-tokyo.ac.jp

[†] Japan Aerospace Exploration Agency (JAXA)
Yoshinodai Chuo-ku Sagamihara-shi 252-5210 Kanagawa, Japan
e-mail: oyama@flab.isas.jaxa.jp
e-mail: maru.yusuke@jaxa.jp

[‡]Teikyo University
1-1 Toyosatodai Utsunomiya-shi 320-8551 Tochigi, Japan
e-mail: manako@ase.teikyo-u.ac.jp

Key words: Air-breathing rocket, Coaxial nozzle, CFD

Summary. It is anticipated that the rocket-based combined cycle engine, which incorporates a rocket engine and an airbreathing engine, will offer enhanced propulsive capabilities compared to conventional rocket engines. The exhaust nozzle is a coaxial nozzle comprising a convergent-divergent nozzle in the center and a convergent nozzle around it. This represents an unprecedented configuration for a rocket engine nozzle. The objective of this study is to numerically analyze the flow field near the nozzle exit and to elucidate the impact of jet interference on thrust to facilitate the detailed design of rockets. In this study, an airbreathing sounding rocket, currently under research and development at JAXA, is employed as the analysis target. The resulting calculation yielded the flow field data around the nozzle. When the central jet is over-expanded, the velocity and pressure distributions at the nozzle outlet undergo alterations due to the mutual effect of one jet pulling in the other jet. The combined thrust of the two nozzles activated simultaneously was found to be lower than the sum of the individual thrusts of the two cases in which only one of the nozzles was activated. Conversely, the thrust remains constant when the central jet is under-expanded.

1 INTRODUCTION

In recent years, research and development of space vehicles with lower costs and higher efficiencies have been actively conducted to meet the increasing demand for transportation. Concerning the propulsion system, it is anticipated that a rocket-based combined cycle system, which incorporates a rocket engine (RE) in conjunction with an air-breathing engine (ABE), will prove to be a revolutionary technology capable of transcending the performance constraints of the conventional RE. This is because it can substitute a proportion of the onboard oxidizer with oxygen drawn from the atmosphere during intake [1]. To illustrate, consider a reusable

sounding rocket equipped with a rocket-based combined cycle engine, as depicted in Figure 1. The subject is currently undergoing research and development at the Japan Aerospace Exploration Agency (JAXA) and is the focus of analysis in this study [2]. The use of the ABE with a higher specific impulse than the RE during both launch and landing enables the rocket to achieve high propulsion performance. However, the ABE is unable to generate sufficient thrust at high altitudes with low density. The combination of the RE helps the rocket achieve the necessary thrust for ascent. Consequently, at certain altitudes, both the RE and ABE are employed in parallel.

The present study is concerned with the exhaust nozzle, which is one of the engine components that exerts a significant influence on the thrust of a rocket. Given the simplicity of the configuration, the rocket employs a design in which the RE is situated in the center and the ABE is positioned around it. The nozzle exit plane is of a double cylindrical shape (i.e., a coaxial nozzle), as illustrated in Figure 2. This configuration is also employed by the SABRE [3]. In the case of a rocket with two engines operating simultaneously, three distinct flows with varying velocities are observed, as illustrated in Figure 3. The initial flow is a supersonic jet ejected from a convergent-divergent nozzle of the RE, situated in the center. The second is a sonic jet ejected from a convergent nozzle of the ABE on the periphery. The third flow is the external flow, which has the same speed as the rocket in the opposite direction.

The coaxial jet has been the subject of considerable interest and a substantial body of research has been conducted on the topic. However, given that the use of a coaxial nozzle as a rocket engine exhaust nozzle is without precedent, there is a paucity of knowledge regarding the thrust generated by coaxial nozzles. As an illustration of a study that suggests an effect on thrust, Lovaraju et al. [4] conducted experiments that demonstrated that the potential core of the central jet, extending from the nozzle outlet, is elongated by the presence of the surrounding jet in a quiescent fluid. This phenomenon occurs when the central jet is correctly expanded and under-expanded. Sharma et al. [5] demonstrated that the pitot pressure distribution at the nozzle exit is altered by the presence of the surrounding jet and that the shock wave structure of the central jet is modified when the central jet is over-expanded in a quiescent fluid. Samara et al. [6] conducted a numerical analysis and experimental investigation to examine the impact of interference between a central and surrounding supersonic jet on propulsive performance in supersonic flow. It was thus determined that when the Mach number of the central jet is less than that of the surrounding jets, the thrust increases due to the interference of the jets. Conversely, when the Mach number of the central jet is greater than that of the surrounding jets, the thrust decreases due to the interference of the jets.

As evidenced by prior research, the interference effects of jets are likely to impact the thrust generated by nozzles. In the field of rocket design, it is of paramount importance to accurately estimate the change in thrust in advance, as this directly correlates with the amount of payload and fuel that can be carried. The objective of this study is to conduct a numerical analysis of the flow field surrounding the nozzle and to evaluate the quantitative impact of the interference of the coaxial jet on the actual operational flow conditions of the rocket.

Figure 1: Air-breathing rocket

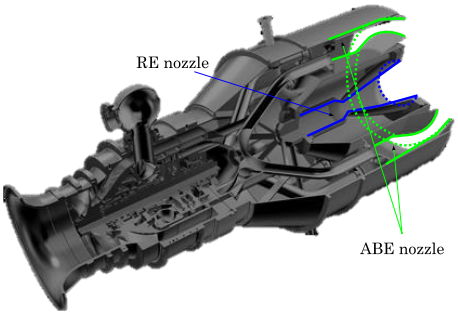

Figure 2: ATRIUM engine

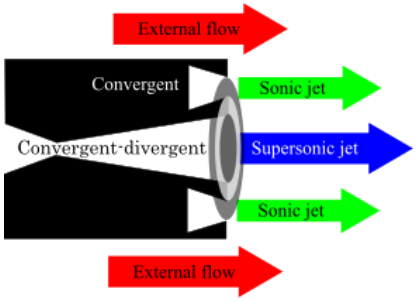

Figure 3: Schematic of the flow field around the nozzle

2 APPROACHES

2.1 Analysis model

The analysis model presented in this study is a representation of the rear portion of the rocket, as illustrated in Figure 4. The cross-sectional view of the model is illustrated in Figure 5. The center convergent-divergent nozzle of the RE has a throat diameter of $D_{rt} = 0.066$ [m] and an exit diameter of $D_r = 0.201$ [m]. The ratio of the exit plane area to the throat area is 9.24. The contour of the nozzle was designed by the methods of the compressed truncated perfect nozzle, as outlined in reference [7]. A quasi-one-dimensional approximation of the flow indicates that the nozzle pressure ratio (NPR) at the correct expansion is 121.6. It should be noted that the NPR is defined as the ratio of the chamber pressure to the ambient pressure.

The cross-section of the surrounding convergent nozzle of ABE is annular in shape, and the difference between the inner and outer diameters of the exit plane is $D_{at} = 0.072$ [m]. The area ratio of the inlet plane area to the outlet plane area is 0.67. The NPR at the correct expansion is 1.667.

The distance between the tip of the RE nozzle and the inner tip of the ABE nozzle at the exit plane is $0.221D_r$. The outer surface of the ABE exhibits a wall thickness of $0.0149D_r$. The ABE nozzle is tapered at a rate of 15 degrees from both sides. The aft portion of the rocket surface assumes a boat-tail configuration along the tapered section of the ABE nozzle.

In this study, the origin of the coordinate system is defined as the center of the nozzle exit plane of the RE. The direction of the coordinate axes is defined as follows: the x-axis is

coincident with the nozzle center axis and positive in the direction opposite to the direction of rocket travel; the z-axis is positive in the radial direction; and the y-axis is perpendicular to these two axes.

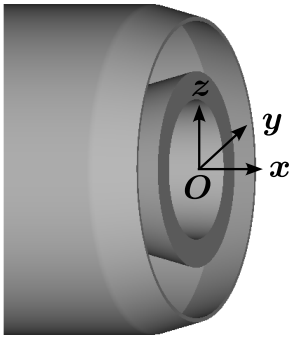

Figure 4: Analysis model

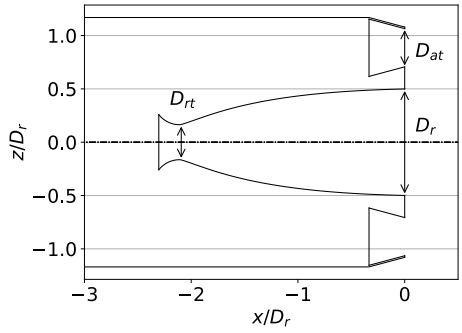

Figure 5: Cross-sectional view of the nozzles

2.2 Flow conditions

Two points were selected from the ascent trajectory obtained using a one-dimensional vertical simulation [8] shown in Figure 6 to emulate the actual operational conditions of the rocket under analysis. In this trajectory, the rocket ascends solely with ABE for the initial 30 seconds post-launch, subsequently transitioning to RE and climbing with both engines in operation. Given that the chamber pressure of the nozzle remains constant while the ambient pressure declines with ascent, the NPR consequently increases. The RE jet expands correctly at an altitude of 78 seconds after launch; however, at lower altitudes, it over-expands, and at higher altitudes, it under-expands. In this analysis, the flow conditions at the altitude of 30 seconds after launch, which corresponds to the point at which the RE jet over-expands, and at the altitude of 90 seconds after launch, which corresponds to the point at which the RE jet under-expands, were utilized. The pertinent flow conditions at the two points are presented in Table 1. The Reynolds number was calculated using the RE nozzle exit diameter as the characteristic length and the RE jet velocity at the exit as the characteristic velocity.

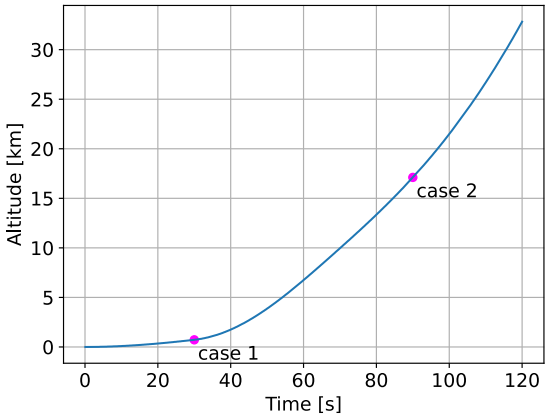

Figure 6: Reference trajectory

Table 1: Flight and flow field conditions

Parameter	Unit	Case 1	Case 2
Mach number of external flow M_∞		0.485	1.37
Pressure of external flow p_∞	MPa	0.082	0.0089
Density of external flow ρ_∞	kg/m^3	1.04	0.144
Nozzle pressure ratio (NPR) of RE		41.4	382
Nozzle pressure ratio (NPR) of ABE		2.07	5.26
Reynolds number		1.3×10^5	2.3×10^5

2.3 Computational methods

In this study, numerical simulations were conducted using the in-house code, LANS3D, developed by Fujii et al. [9, 10], to analyze the flow field around the nozzles. The fundamental equations are three-dimensional compressible Navier-Stokes equations. The convective flux was calculated using the simple high-resolution upwind scheme (SHUS) and the third-order monotone upstream scheme for the conservation law (MUSCL). The alternating direction iteration symmetric Gauss-Seidel method (ADI-SGS) was employed for the time integration process. The data utilized in this study were averaged following the attainment of a steady flow field. The viscous terms were evaluated using a second-order accurate central differencing scheme, and the eddy viscosity was modeled using the Baldwin-Lomax turbulence model [14], based on the results of validations of the simulation with several models against the experimental data.

2.4 Computational mesh

The computational mesh used in this study is shown in Figure 7. It is assumed that the flow field around the nozzle is axisymmetric about the x-axis. Consequently, the computational domain has a fan-shaped cross-section with a central angle of twenty degrees. The domain was defined with dimensions of $5D_r$ upstream from the nozzle exit, $30D_r$ downstream from the nozzle exit, and $20D_r$ in the radial direction. The computational domain was divided into the RE and ABE nozzles, as well as the upstream and downstream regions from the nozzle exit. The values were then exchanged between these domains. The number of grid points utilized for each domain is presented in Table 2. The number of grid points was determined based on the findings of the grid dependency study. The minimum grid size was determined to ensure that at least one or more grid points are situated within the viscous sublayer.

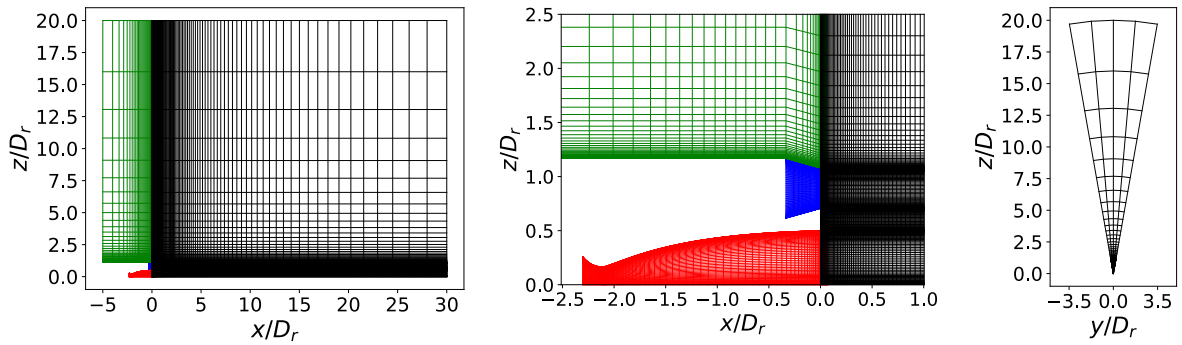

(a): Overview **(b)**: Around the nozzle exit **(c)**: Cross-section

Figure 7: Computational grid

Table 2: Details of the number of grid points

Domain name	N_x	N_y	N_z	Total
RE nozzle (red)	92	5	90	41400
ABE nozzle (blue)	48	5	100	24000
External upstream (green)	38	5	70	13300
External downstream (black)	108	5	396	213840

2.5 Boundary conditions

The inner wall of the nozzles and the surface of the rocket were all considered adiabatic viscous walls. The nozzle outlet, which is not used in the stand-alone operation condition, was blocked and treated as a viscous wall. The downstream end and sides of the computational domain were treated as outflow conditions. The upstream end outside the rocket was given a uniform inflow condition of velocity u_∞ in the x direction. The inlet of the nozzles was given uniform pressure NPR $\times$ p_∞ and temperature. The grid points on the nozzle center axis were extrapolated to the average of the values of the surrounding grid points.

2.6 Evaluation method

The thrust F generated by the nozzles is decomposed into a momentum thrust F_m and a pressure thrust F_p as shown in equation (1). Each part of thrust was obtained from the distribution of the flow velocity u_e, density ρ_e, and pressure p_e at the nozzle exit (area A_e) by integrating them as in equation (2). The pressure thrust was obtained by integrating the difference of the nozzle outlet pressure from the ambient pressure p_∞.

$$F = F_m + F_p \tag{1}$$

$$= \int_{A_e} \rho_e u_e^2 dA + \int_{A_e} (p_e - p_\infty) dA \tag{2}$$

To elucidate the interference effect of coaxial jets, three operational modes for each flow condition were analyzed: (A) the RE and ABE operate simultaneously, (B) the RE operates alone, and (C) the ABE operates alone. If the sum of the thrust generated by the RE and ABE nozzles in mode (A) is greater than or less than the sum of the thrust generated by the RE nozzle in mode (B) and the ABE nozzle in mode (C), the interference effect of the jets contributes to

an improvement or deterioration in the performance of the thrust of the nozzles.

3 RESULTS

3.1 Jets interference effect on thrust in case 1

Figure 8 illustrates the outcomes of a comparative analysis of the RE thrust F^r between mode (A) and mode (B), and the ABE thrust F^a between mode (A) and mode (C). Furthermore, the sum of the thrust of the RE and ABE at mode (A), and the sum of the thrust of the RE obtained at mode (B) and the ABE obtained at mode (C) are presented. The former sum of the thrust from each nozzle was found to be 1.15% less than the latter. A reduction of 2.75% was observed in the RE thrust when comparing mode (A) to mode (B). Conversely, the ABE thrust was observed to increase by 0.80% in the case of mode (A) compared to the case of mode (C). These results suggest that the RE thrust is degraded by the presence of the surrounding ABE jet, while the ABE thrust is enhanced by the presence of the central RE jet. As the reduction in the thrust of the RE nozzle exceeds the increase in the thrust of the ABE nozzle, the combined thrust of the coaxial nozzle is adversely affected by the interference of the jets when the RE nozzle is over-expanded.

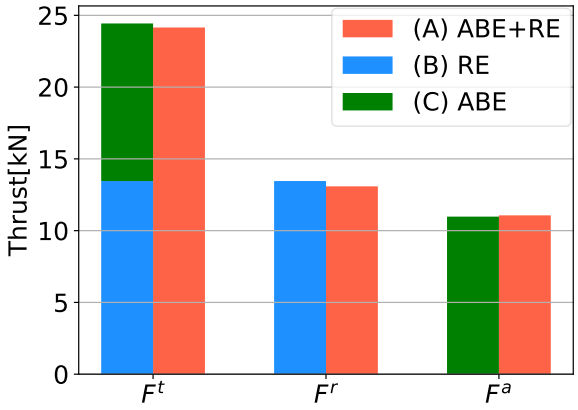

Figure 8: Comparison of the thrust between simultaneous and individual operation in case 1

3.2 The breakdown of the decreased RE thrust and the increased ABE thrust

The thrust generated by each nozzle can be decomposed into two distinct components: momentum thrust and pressure thrust. This is illustrated by the equation (1). This section addresses the impact of jet interaction on the momentum and pressure thrust. Figure 9 illustrates the comparison of the momentum thrust F_m^r and pressure thrust F_p^r of the RE between the case of simultaneous operation and independent operation. Mode (A) exhibited a 1.73% increase in momentum thrust compared to mode (B). The pressure thrust was negative as a result of the jet of the RE being over-expanded. In comparison to mode (B), the pressure thrust of mode (A) exhibited a reduction. The reduction in the pressure thrust exceeded the augmentation in the momentum thrust, resulting in a decline in the RE thrust.

Figure 10 illustrates the comparison of the momentum thrust F_m^a and pressure thrust F_p^a of the ABE between the cases of simultaneous operation and independent operation. In

comparison to mode (C), mode (A) exhibited an increase of 4.50% in its momentum thrust, while simultaneously displaying a decrease of 14.9% in its pressure thrust. The augmentation in pressure thrust exceeded the diminution in momentum thrust, thereby precipitating an increase in the ABE thrust.

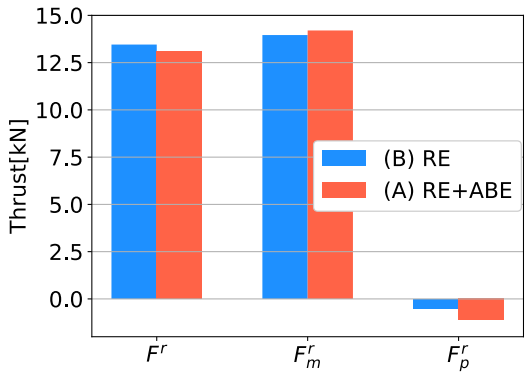

Figure 9: Breakdown of RE thrust

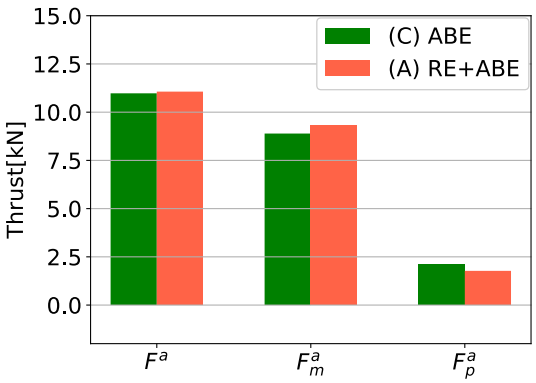

Figure 10: Breakdown of ABE thrust

3.3 Changes in flow field around the nozzle in case 1

The exit state of the nozzle determined the thrust generated by the nozzle. The momentum thrust is primarily influenced by the velocity profile u, which is parallel to the x-axis. In contrast, the pressure thrust is determined by the pressure profile p at the nozzle exit plane. The distributions were found to be influenced by alterations in the flow field surrounding the nozzle.

Figure 11 illustrates the velocity u and pressure profiles at the nozzle exit. All velocity and pressure profiles and distributions shown in this paper are normalized by the sound velocity and pressure of the external flow, respectively. Each graph presents two profiles, one for simultaneous operation and one for individual operation. As illustrated in Figure 11a and Figure 11b, a comparison of modes (A) and (B) reveals that, from a distance of $0.2D_r$ from the nozzle center to the edge of the RE nozzle, there is an increase in velocity and a corresponding decrease in pressure for mode (A). As illustrated in Figure 11c and Figure 11d, the velocity increased and the pressure decreased at mode (A) in comparison to mode (C). The discrepancy between the two modes was most pronounced at the inner tip of the ABE nozzle ($z/D_r = 0.706$). The observed increase in velocity and decrease in pressure increased momentum thrust and a decrease in pressure thrust, respectively.

The distributions of velocity and pressure are illustrated in Figure 12. A negative pressure region, which was surrounded by the jets from the RE and ABE nozzles, appeared in Figure 12b corresponding to mode (A), although it was not present in Figure 12d, corresponding to mode (B). The RE jet within the nozzle was influenced by the negative pressure region, resulting in a downstream shift of the separation point observed in comparison to mode (B) (Figure 12a and Figure 12c). This led to an increase in the area occupied by the RE jets at the nozzle exit plane. In contrast, a comparison of Figure 12b at mode (A) and Figure 12f at mode (C) indicates that the pressure near the inner nozzle rip of the ABE at mode (A) was a little lower than that at mode (C), resulting in a reduction in pressure at the inner nozzle rip as shown in the profile.

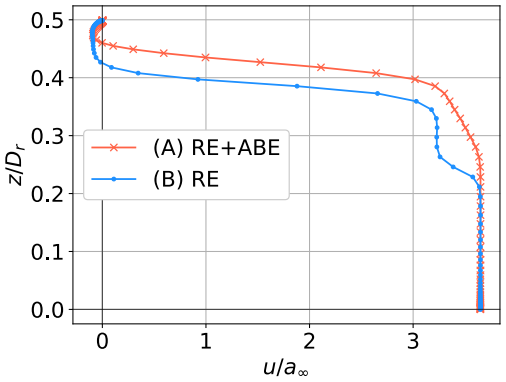

(a): Velocity u at RE nozzle exit

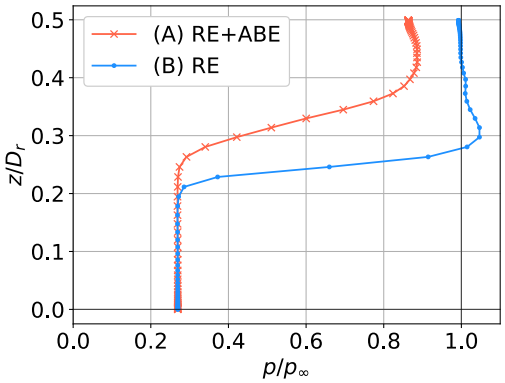

(b): Pressure at RE nozzle exit

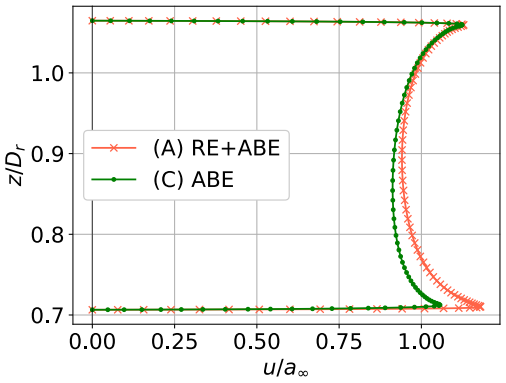

(c): Velocity u at ABE nozzle exit

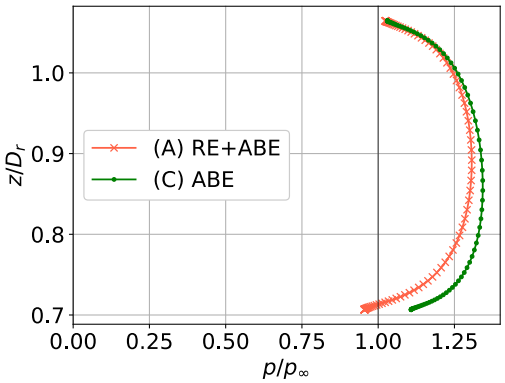

(d): Pressure at ABE nozzle exit

Figure 11: Profiles of nozzle exit in case 1

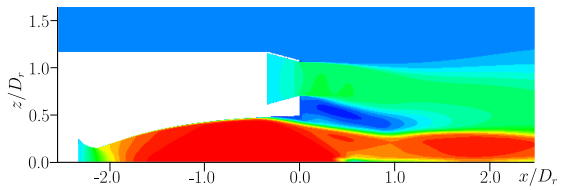

(a): Velocity u distribution at mode (A)

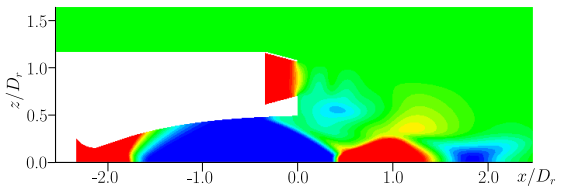

(b): Pressure distribution at mode (A)

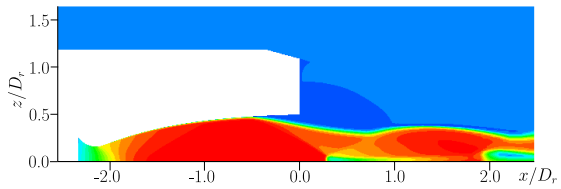

(c): Velocity u distribution at mode (B)

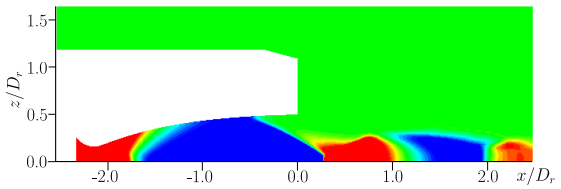

(d): Pressure distribution at mode (B)

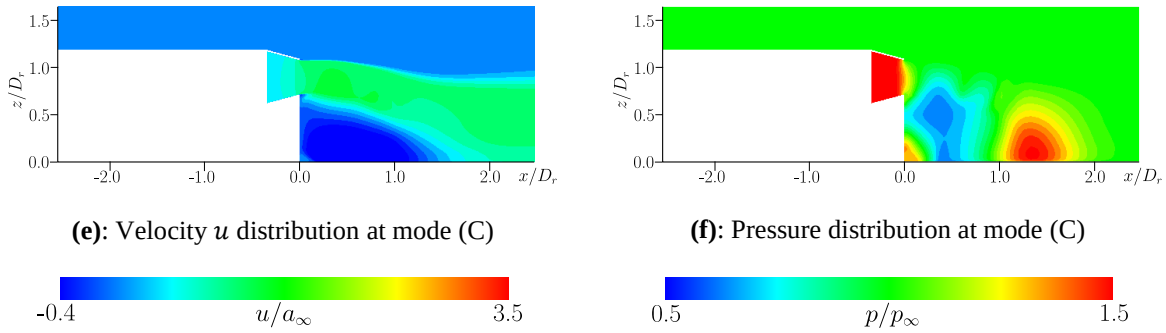

(e): Velocity u distribution at mode (C)

(f): Pressure distribution at mode (C)

Figure 12: Flow field around the nozzle in case 1

3.4 Jet interference effect on thrust in case 2

The thrust type illustrated in Figure 13 is identical to that depicted in the preceding section. The types of thrust, including the RE, ABE, and total thrust, remained unaltered between the simultaneous and independent operation cases. It can thus be concluded that the interference effect has no impact on the total thrust of the coaxial nozzle when the central RE jet is under-expanded.

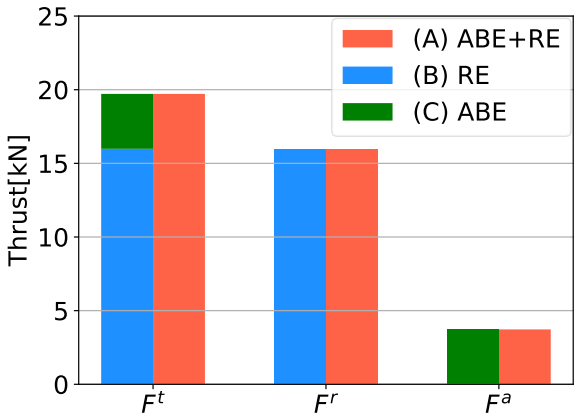

Figure 13: Comparison of the thrust between simultaneous and individual operation in case 2

3.5 Changes in flow field around the nozzle in case 2

Figure 14 illustrates the velocity u and pressure profiles at the nozzle exit. Each graph presents two profiles, one for simultaneous operation and one for individual operation. The profiles of the two nozzles remained identical when operated in either mode. However, the flow field surrounding the nozzle exit transformed, as illustrated in Figure 15. The impact of alterations in velocity and pressure distribution did not extend to the nozzle exit and internal regions when the jet from each nozzle was under-expanded.

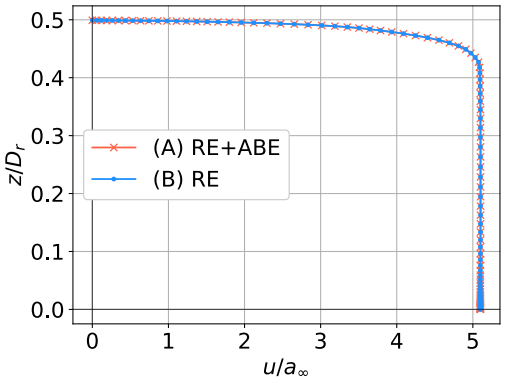

(a): Velocity u at RE nozzle exit

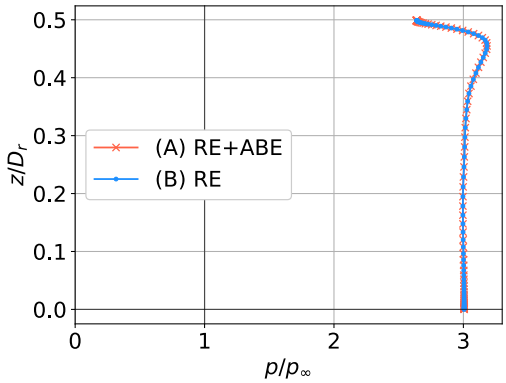

(b): Pressure at RE nozzle exit

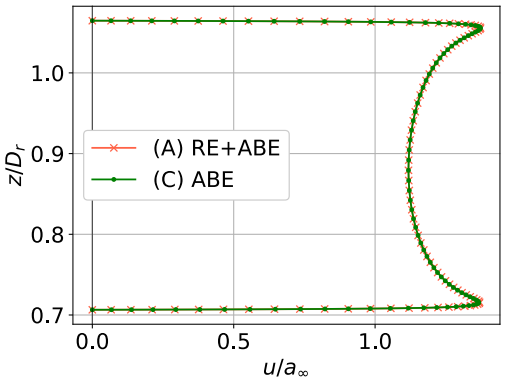

(c): Velocity u at ABE nozzle exit

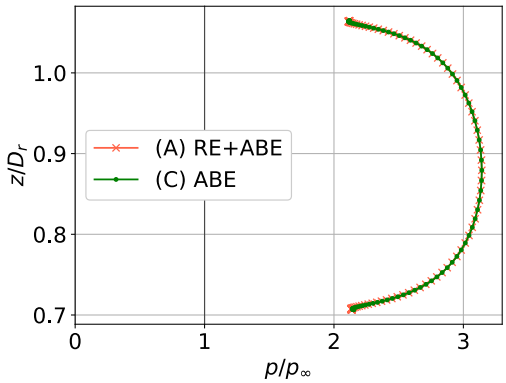

(d): Pressure at ABE nozzle exit

Figure 14: Profiles of nozzle exit in case 2

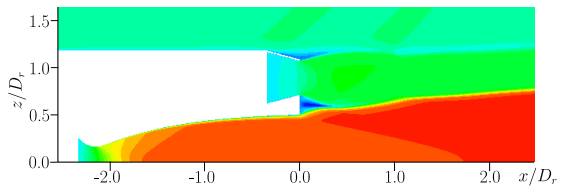

(a): Velocity u distribution at mode (A)

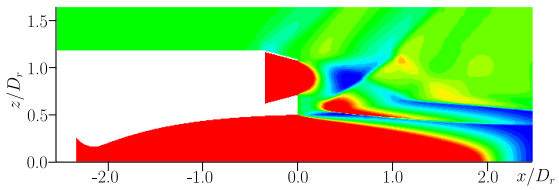

(b): Pressure distribution at mode (A)

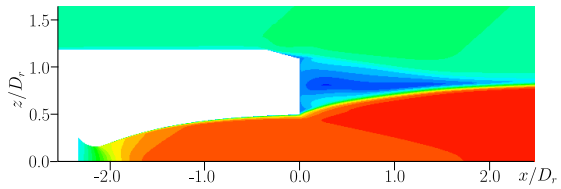

(c): Velocity u distribution at mode (B)

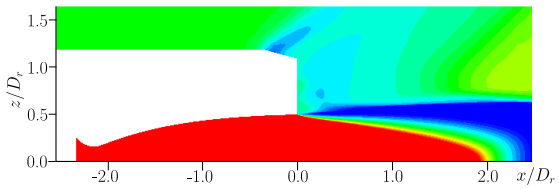

(d): Pressure distribution at mode (B)

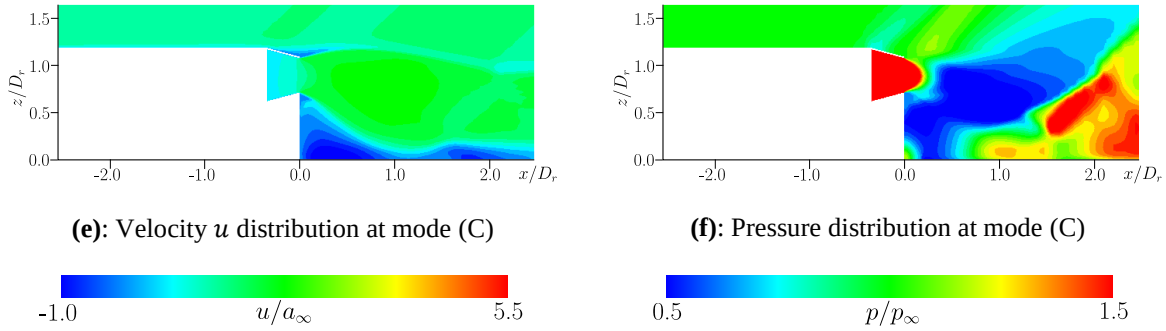

(e): Velocity u distribution at mode (C)

(f): Pressure distribution at mode (C)

Figure 15: Flow field around the nozzle in case 2

4 CONCLUSIONS

The objective of this study was to quantitatively investigate the effect of interference between two jets of a coaxial nozzle with a convergent-divergent nozzle in the center and a convergent nozzle around it on thrust under the flight condition of the air-breathing rocket. Two cases were selected for analysis, one in which the RE jet is over-expanded and the other in which it is under-expanded.

1. In the case where the RE jet is over-expanded (case 1), the jets' interaction effect resulted in a 1.13% reduction in the total thrust generated from the coaxial nozzle. This was due to the decrease in the thrust of the RE exceeding the increase in the thrust of the ABE between the simultaneous and individual operation for each engine. The velocity profiles parallel to the x-axis and pressure distributions indicated that velocity increased and pressure decreased at the nozzle tip in proximity to the other nozzle.
2. In the case of an under-expanded RE jet (case 2), the jets' interaction effect did not result in any discernible impact on the thrust generated by the nozzle. Despite alterations in the distribution of velocity and pressure, the profiles themselves remained unaltered.

It can be reasonably deduced that in the actual flight of a rocket, the thrust may be decreased due to the interference effect of the coaxial nozzles at the altitude where the central RE jet is over-expanded. In the design of a rocket with a coaxial nozzle as an exhaust nozzle, it is inadvisable to estimate the thrust as the sum of the thrust generated from each nozzle in advance. Rather, the design should proceed with consideration of the interference effect on thrust.

REFERENCES

[1] H. Kobayashi, Y. Maru, Richardson, M. P., K. Kinefuchi, and T. Sato. 2021. “Conceptual design study of a vertical takeoff and landing airbreather.” *Journal of Spacecraft and Rockets* 58, No. 5: 1279–1292. https://doi.org/10.2514/1.A34988

[2] T. Sato, H. Taguchi, and H. Kobayashi. 2021. “Development Status of Air-Breathing Engines for Space Transport.” In *Proceedings of Space Transportation Symposium FY2020*. In Japanese. http://id.nii.ac.jp/1696/00047574/

[3] Mehta, U. B., Aftosmis, M. J., Bowles, J. V., and Pandya, S. A. 2015. “Skylon aerodynamics and SABRE plumes.” In *20th AIAA International Space Planes and*

Hypersonic Systems and Technologies Conference. https://doi.org/10.2514/6.2015-3605

[4] Lovaraju, P., and Rathakrishnan, E. 2011. "Experimental studies on co-flowing subsonic and sonic jets." *Flow, turbulence, and combustion* 87: 115–132. https://doi.org/10.1007/s10494-011-9332-5

[5] Sharma, H., Vashishtha, A., Rathakrishnan, E., Lovaraju, P. 2008. "Experimental study of overexpanded co-flowing jets." *The Aeronautical Journal* 112, No. 1135: 537–546. https://doi.org/10.1017/S0001924000002499

[6] Samara, M. S., Vashishtha, Y. Watanabe, and K. Suzuki. 2020. "Flow-field and performance study of coaxial supersonic nozzles operating in hypersonic environment." *International Review of Aerospace Engineering* 13, No. 1: 25–39. https://doi.org/10.15866/irease.v13i1.18282

[7] Hoffman, J. D. 1987. "Design of compressed truncated perfect nozzles." *Journal of propulsion and power* 3, No. 2: 150–156. https://doi.org/10.2514/3.22967

[8] T. Saito, A. Oyama, H. Kobayashi, and Y. Maru. 2019. "Study on Multi-objective Design Optimization of Air Breathing Engine Fan for Sounding Rocket." In *Design and Systems Conference*. In Japanese. https://doi.org/10.1299/jsmedsd.2019.29.1205

[9] S. Obayashi, K. Kuwahara, and K. Fujii. 1986. "Improvements in Efficiency and Reliability for Navier-Stokes Computations Using the LU-ADI Factorization Algorithm." In *24th Aerospace Science Meeting*: 338. https://doi.org/10.2514/6.1986-338

[10] K. Fujii. 1990. "Developing an Accurate and Efficient Method for Compressible Flow Simulations – An Example of CFD in Aeronautics." In *Proceedings of Fifth International Conference on Numerical Ship Hydrodynamics* 1: 1–17.

[11] E. Shima, and T. Jounouchi, 1997. "Role of CFD in Aeronautical Engineering (No. 14) - AUSM Type Upwind Schemes." In *Proceeding of the 14th NAL Symposium on Aircraft Computational Aerodynamics*: 7–12.

[12] Van Leer, B., 1977. "Towards the Ultimate Conservative Difference Scheme. IV. A New Approach to Numerical Convection." *Journal of Computational Physics* 23. No. 3: 276–299. https://doi.org/10.1016/0021-9991(77)90095-X

[13] H. Nishida, and T. Nonomura, 2009. "ADI-SGS Scheme on Ideal Magnetohydrodynamics." *Journal of Computational Physics* 228. No. 9: 3182–3188. https://doi.org/10.1016/j.jcp.2009.01.032

[14] Baldwin, B., and Lomax, H., 1978. "Thin-Layer Approximation and Algebraic Model for Separated Turbulentflows." In *16th aerospace sciences meeting*: 257. https://doi.org/10.2514/6.1978-257